



*Supplement of*

**Modeling the interinfluence of fertilizer-induced NH<sub>3</sub> emission, nitrogen deposition, and aerosol radiative effects using modified CESM2**

**Ka Ming Fung et al.**

*Correspondence to:* Ka Ming Fung ([kamingfung@link.cuhk.edu.hk](mailto:kamingfung@link.cuhk.edu.hk)), Maria Val Martin ([m.valmartin@sheffield.ac.uk](mailto:m.valmartin@sheffield.ac.uk)), and Amos P. K. Tai ([amostai@cuhk.edu.hk](mailto:amostai@cuhk.edu.hk))

The copyright of individual parts of the supplement might differ from the article licence.

## Supplementary Information

### 1. Soil structure

**Table S1. Soil layer structure.**

Layer#	Layer Node Depth $l$ (m)	Layer Thickness $\Delta l$ (m)	Weighting Factor $e^{(-10l)/\Delta l}$	Nitrogen Distribution Fraction
1	0.01	0.02	45.2	62.8%
2	0.04	0.04	16.8	23.3%
3	0.09	0.06	6.8	9.4%
4	0.16	0.08	2.5	3.5%
5	0.26	0.12	0.6	0.9%
6	0.40	0.16	0.1	0.2%
7	0.58	0.20	0.0	-
8	0.80	0.24	0.0	-
9	1.06	0.28	0.0	-
10	1.36	0.32	0.0	-
11	1.70	0.36	0.0	-
12	2.08	0.40	0.0	-
13	2.50	0.44	0.0	-
14	2.99	0.54	0.0	-
15	3.58	0.64	0.0	-
16	4.27	0.74	0.0	-
17	5.06	0.84	0.0	-
18	5.95	0.94	0.0	-
19	6.94	1.04	0.0	-
20	8.03	1.14	0.0	-
21	9.80	2.39	0.0	-
22	13.33	4.68	0.0	-
23	19.48	7.64	0.0	-
24	28.87	11.14	0.0	-
25	42.00	15.12	0.0	-

Reference:

- Section 2.2.2 in CLM5 technical notes, [https://escomp.github.io/ctsm-docs/versions/release-clm5.0/html/tech\\_note/Ecosystem/CLM50\\_Tech\\_Note\\_Ecosystem.html](https://escomp.github.io/ctsm-docs/versions/release-clm5.0/html/tech_note/Ecosystem/CLM50_Tech_Note_Ecosystem.html), accessed on Jul 29, 2021

- Source code of CLM5:  
<https://github.com/ESCOMP/CTSM/blob/master/src/soilbiogeochem/SoilBiogeochemVerticalProfileMod.F90>, accessed on Jul 29, 2021

## 5 2. Canopy capture

**Figure S1** shows the time series of the fractional amount of  $\text{NH}_3$  captured by above-ground crop biomass. Our scheme showed that crops do not capture as much  $\text{NH}_3$  as natural vegetation (~60–80% as estimated in our scheme) due to their smaller canopies, except for sugarcane and temperate soybean, which can retain >30% of  $\text{NH}_3$  emitted. CLM5 allows crops to be irrigated or rainfed. We observed a general trend that irrigated crops retain more soil  $\text{NH}_3$  emission than rainfed ones, which can be explained by their higher in-canopy air humidity. Despite instantaneous values varying with plant growth, our calculated canopy capture fractions are close to those used in previous studies (e.g., Bouwman et al., 1997), i.e., 20% for other shrubs, grasses, and crops.

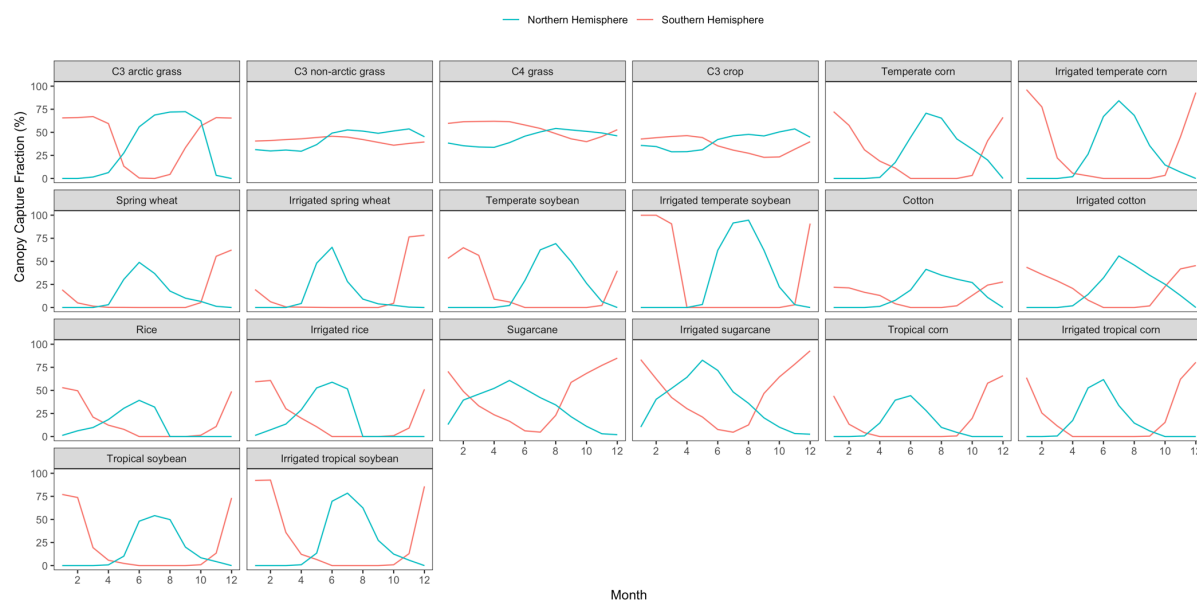


**Figure S1.** Monthly global-mean fractions of  $\text{NH}_3$  captured (%) by each PFT canopy in each hemisphere.

**Table S2. Annual mean fraction of NH<sub>3</sub> captured (%) by PFTs.**

Crops	%NH <sub>3</sub> Captured
Temperate corn	24.8
Irrigated temperate corn	27.1
Spring wheat	12.7
Irrigated spring wheat	14.5
Temperate soybean	19.9
Irrigated temperate soybean	30.1
Cotton	13.2
Irrigated cotton	19.7
Rice	14.3
Irrigated rice	19.0
Sugarcane	37.2
Irrigated sugarcane	41.2
Tropical corn	14.5
Irrigated tropical corn	18.6
Tropical soybean	19.3
Irrigated tropical soybean	25.4

20

### 3. Sensitivity to soil pH

CLM5 does not have a built-in method to compute soil pH implicitly. Thus, in **Results**, we used a constant global pH of 6.5, based on the implementation of the NH<sub>3</sub> volatilization scheme in DNDC (Li et al., 2012), to avoid the uncertain and highly spatial varying soil acidity. We tested the sensitivity of our simulated NH<sub>3</sub> emission by using the soil pH map from the Harmonized World Soil Database (HWSD) v1.2 (Wieder, 2014) showed in **Figure S2(c)**. This soil pH dataset shows that the middle 50% of soil has pH values ranged from 5.4–7.0. When comparing maps in **Figure S2(b)** and **(c)**, we observed that the more alkaline the soil is, the more soil emits NH<sub>3</sub>. From our scheme (**Eq. (3)** in particular) for NH<sub>3</sub> volatilization, the emission rate is of the order of 10<sup>pH</sup>:

30

$$F_{\text{soil,pot}} \sim O\left(\frac{K_w}{10^{-\text{pH}K_a}}\right) \sim O'(10^{\text{pH}}) \quad (\text{S1})$$

**Figure S2(d)** also illustrates and confirms this exponential relation between NH<sub>3</sub> emission and pH, pointing to a demand for an implicit approach for calculating prognostic soil alkalinity. Current version of CLM5 tracks only a few chemicals in soil, including NH<sub>4</sub><sup>+</sup>, NO<sub>3</sub><sup>-</sup>,

and methane ( $\text{CH}_4$ ), making the calculation of bulk soil pH difficult. Future models shall include crucial chemicals and processes, as characterized by experimental studies, that affect soil pH.

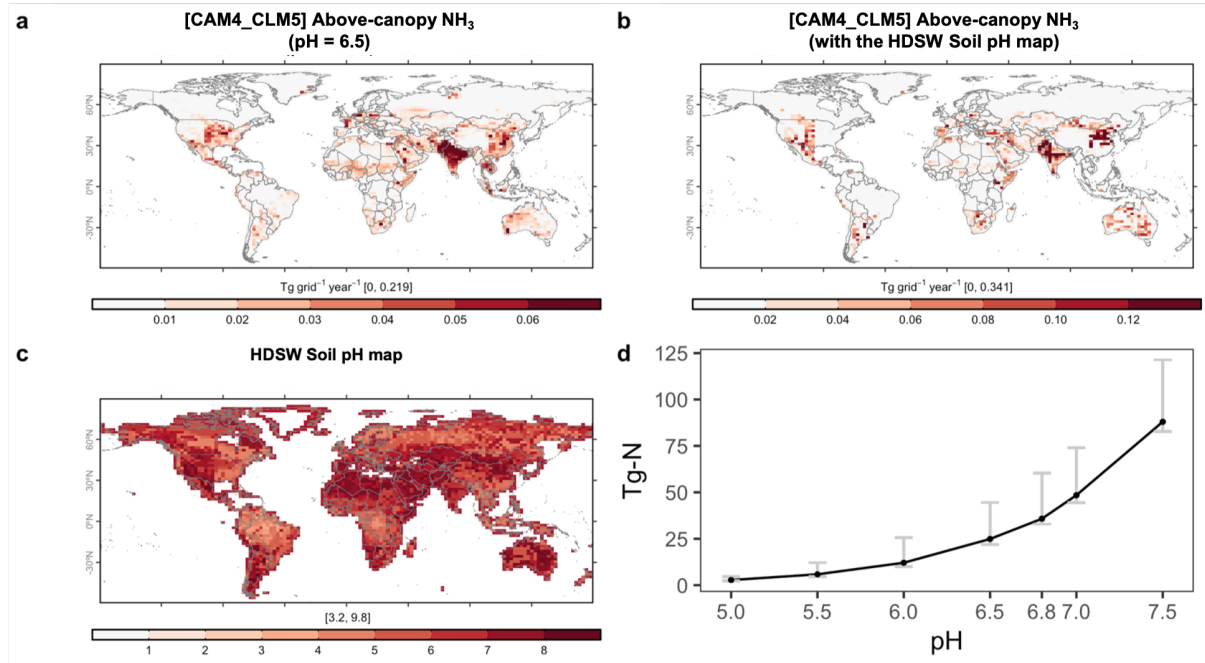


**Figure S2.** CLM5-simulated global soil  $\text{NH}_3$  emission at above-canopy level with (a) a constant global pH of 6.5, and; (b) a spatially varying pH map re-gridded from the Harmonized World Soil Database v1.2 (HWSD) (Wieder, 2014), which is shown in map (c). Graph (d) shows the total soil  $\text{NH}_3$  emission against various global pH values from 5.0 to 7.5. Error bars indicate the maxima and minima across five of simulation.

#### 4. Modifications to CLM5 for modeling other reactive nitrogen

In addition to the  $\text{NH}_3$  schemes, we also incorporated new equations to calculate  $\text{NO}_x$  released as by-products of nitrification and denitrification. The original CLM5 estimates the amount of  $\text{N}_2\text{O}$  leakage during nitrification by applying a constant scaling factor to the nitrification rate (Li et al., 2000) while that from denitrification is variable and evaluated by the DayCent approach (Del Grosso et al., 2000). Building on the work of previous studies (Parton et al., 2001, 2004; Zhao et al., 2017), we computed a ratio of  $\text{NO}_x$  to  $\text{N}_2\text{O}$  to account for the leaking of the former during nitrification and denitrification using the following equations:

$$\text{NO}_x:\text{N}_2\text{O} = 15.2 + \frac{35.5 \tan^{-1}[0.68\pi(10D_r-1.86)]}{\pi} \quad (\text{S2})$$

where  $D_r$  is the relative gas diffusivity in soil vs. in air and is calculated as a function of air-filled pore space (AFPS) of soil (Davidson and Trumbore, 1995):

$$D_r = 0.209\text{AFPS}^{\frac{4}{3}} \quad (\text{S3})$$

$$\text{AFPS} = 1 - \frac{\theta_v}{\theta_{v,\text{sat}}} \quad (\text{S4})$$

where  $\theta_v$  and  $\theta_{v,\text{sat}}$  are instantaneous and saturated volumetric soil water content (in  $\text{m}^3 \text{m}^{-3}$ ), respectively.

We also applied a temperature factor to correct the overestimation of  $\text{NO}_x$  emission at high latitudes as suggested in some previous studies (Xu and Prentice, 2008; Zhao et al., 2017):

$$f_T = \min\left(1, e^{308.56\left(\frac{1}{68.02} - \frac{1}{T_{\text{soil}}+46.02}\right)}\right) \quad (\text{S5})$$

where  $T_{\text{soil}}$  is soil temperature measured in Kelvin (K) here.

In addition, we added back the 20% of microbial mineralized nitrogen to the nitrification rate, which was missing in the previous versions of CLM, following the DayCent approach (Parton et al., 2001).

## 5. Supplementary figures to Section 3.2

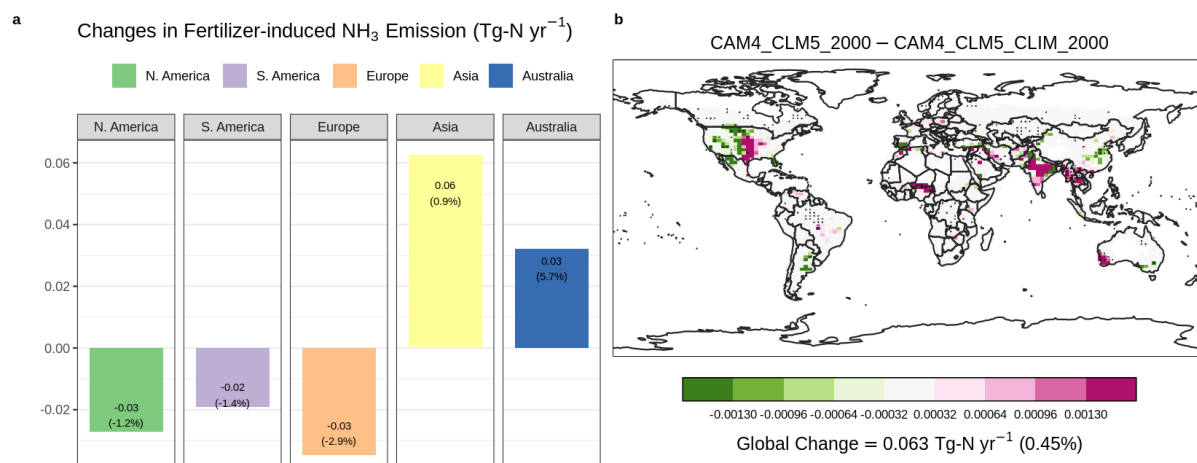


**Figure S3.** Contrasting annual-total fertilizer-induced  $\text{NH}_3$  estimated by fully coupled CAM4-chem with online CLM5  $\text{NH}_3$  emission and  $\text{NH}_y$  deposition ([CAM4\_CLM5\_2000]), and CAM4-chem with online CLM5  $\text{NH}_3$  and prescribed  $\text{NH}_y$  deposition ([CAM4\_CLM5\_CLIM\_2000]) at 2000-level fertilization. The prescribed  $\text{NH}_y$  map in [CAM4\_CLM5\_CLIM\_2000] is from the monthly average of [CAM4\_CLM5\_2000] over 20 years. Panel **(a)** summarizes the regional differences of annual-total  $\text{NH}_3$  emission between the two cases ([CAM4\_CLM5\_2000]–[CAM4\_CLM5\_CLIM\_2000]). Panel **(b)** shows the spatial distribution of their differences.

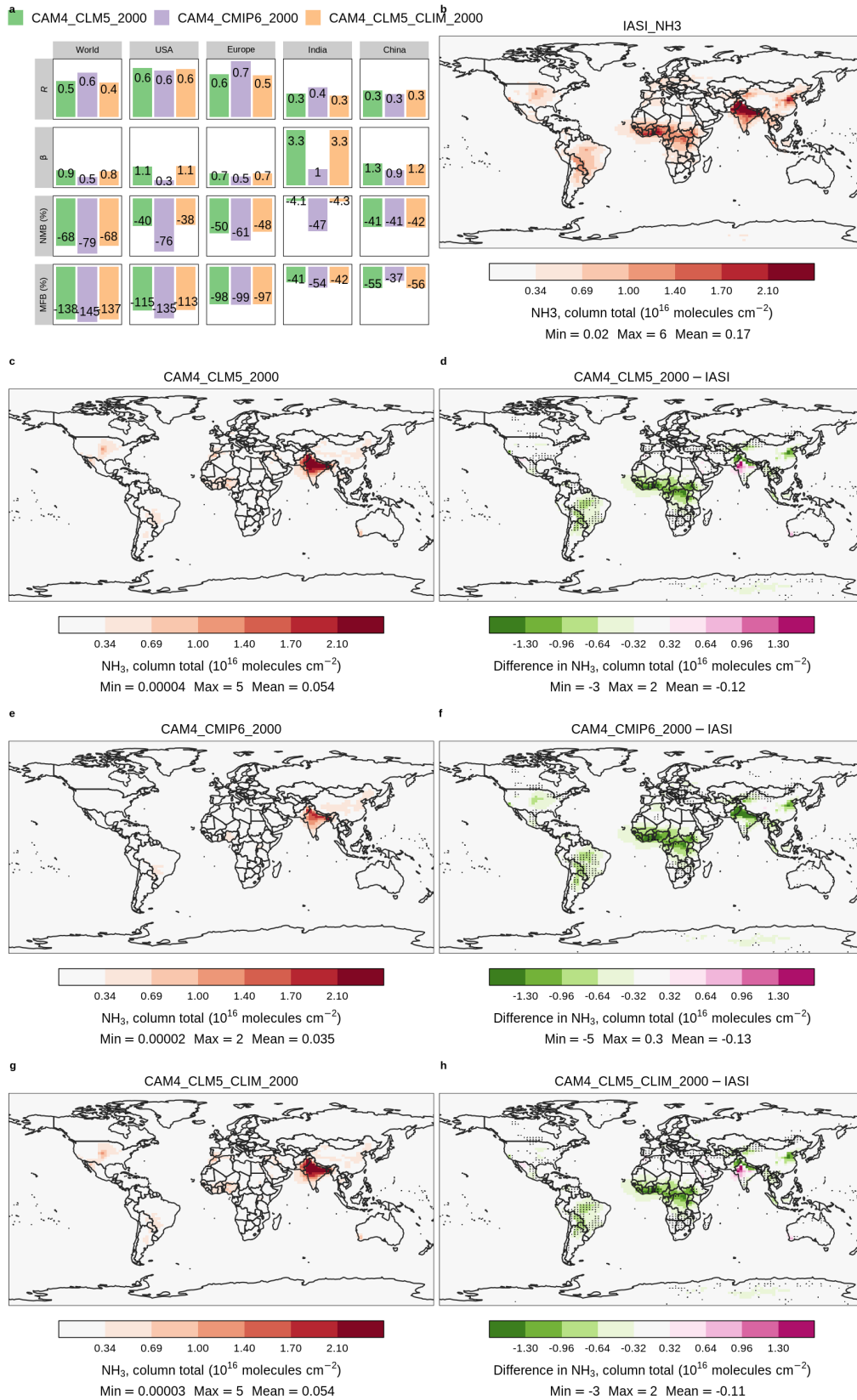


**Figure S4.** Annual-mean atmospheric NH<sub>3</sub> estimated by fully coupled CAM4-chem with online CLM5 NH<sub>3</sub> emission and NH<sub>y</sub> deposition ([CAM4\_CLM5\_2000]), CAM4-chem with fertilizer-induced NH<sub>3</sub> emission from CMIP6 emission inventory and online NH<sub>y</sub> deposition ([CAM4\_CMIP6\_2000]), and CAM4-chem with online



80 CLM5 NH<sub>3</sub> and prescribed NH<sub>y</sub> deposition ([CAM4\_CLM5\_CLIM\_2000]) at 2000-level fertilization. The  
prescribed NH<sub>y</sub> map in [CAM4\_CLM5\_CLIM\_2000] is from the monthly average of [CAM4\_CLM5\_2000] over  
5 years. Panel (a) summarizes correlation analysis between the three cases and the IASI satellite retrievals. Panels  
(b), (c), (e), and (g) show the column NH<sub>3</sub> concentration of IASI and the three simulation cases correspondingly.  
Panels (d), (f) and (h) show concentration differences between each case and the IASI observations. Overlaying  
85 black dots indicate grid-cells with a statistically significant difference under two-sample t-tests (i.e.,  $p < 0.05$ )  
between corresponding simulations. Color scales are saturated at respective values, and ranges of values are shown  
in the legend titles.

## 6. Supplementary figures and table to Section 3.3

**Table S3.** Summary of N fluxes in the simulations averaged over 20 years.

	<b>Fertilization (Tg-N yr<sup>-1</sup>)</b>	<b>Plant Uptake (Tg-N yr<sup>-1</sup>)</b>	<b>Plant Uptake to Fertilization (%)</b>
<b>CAM4_CLM5_2000</b>	96.5	127	132
<b>CAM4_CLM5_2050</b>	117.0	135	115
<b>CAM4_CLM5_CLIM_2050</b>	117.0	133	114
<b>CAM4_CLM5_NDEP_2050</b>	117.0	135	115

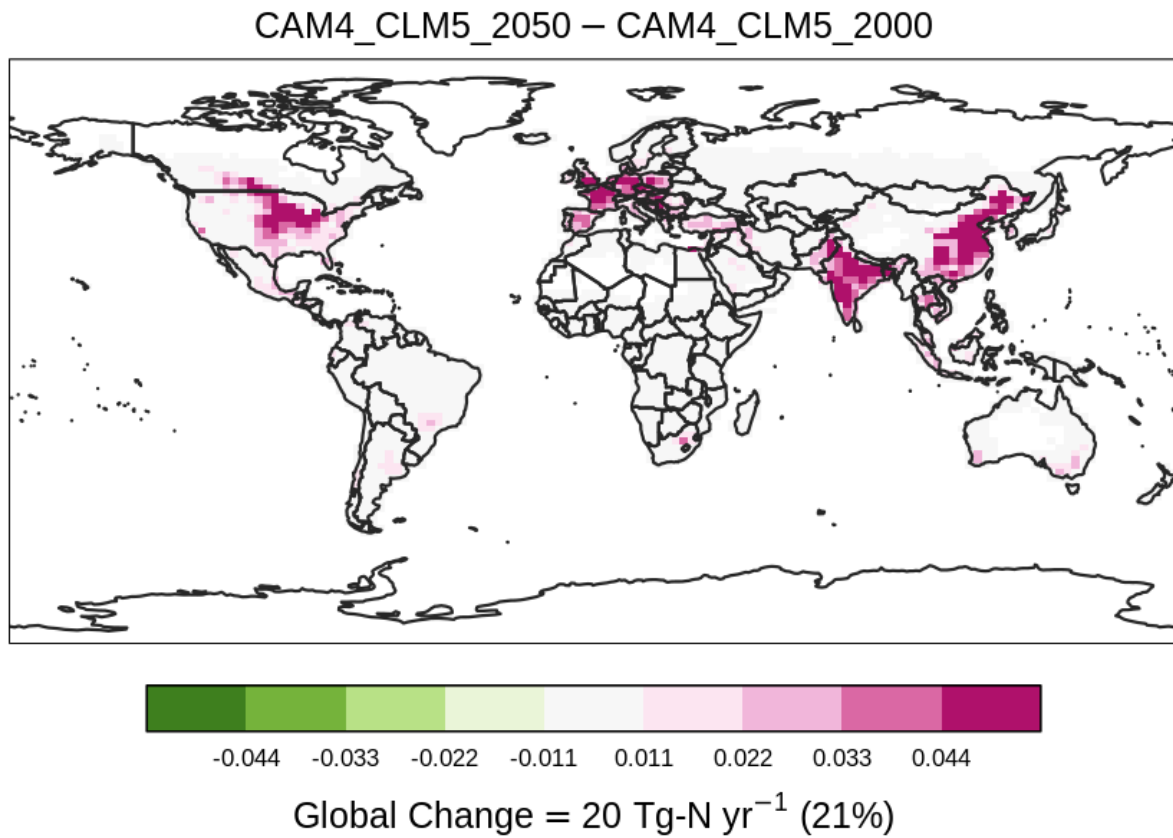


**Figure S5.** Changes in annual-total fertilizer N input to the soil (Tg-N yr<sup>-1</sup>) after an 30% additional synthetic fertilizer is applied from [CAM4\_CLM5\_2000] to [CAM4\_CLM5\_2050]. Color scales are saturated at respective values.

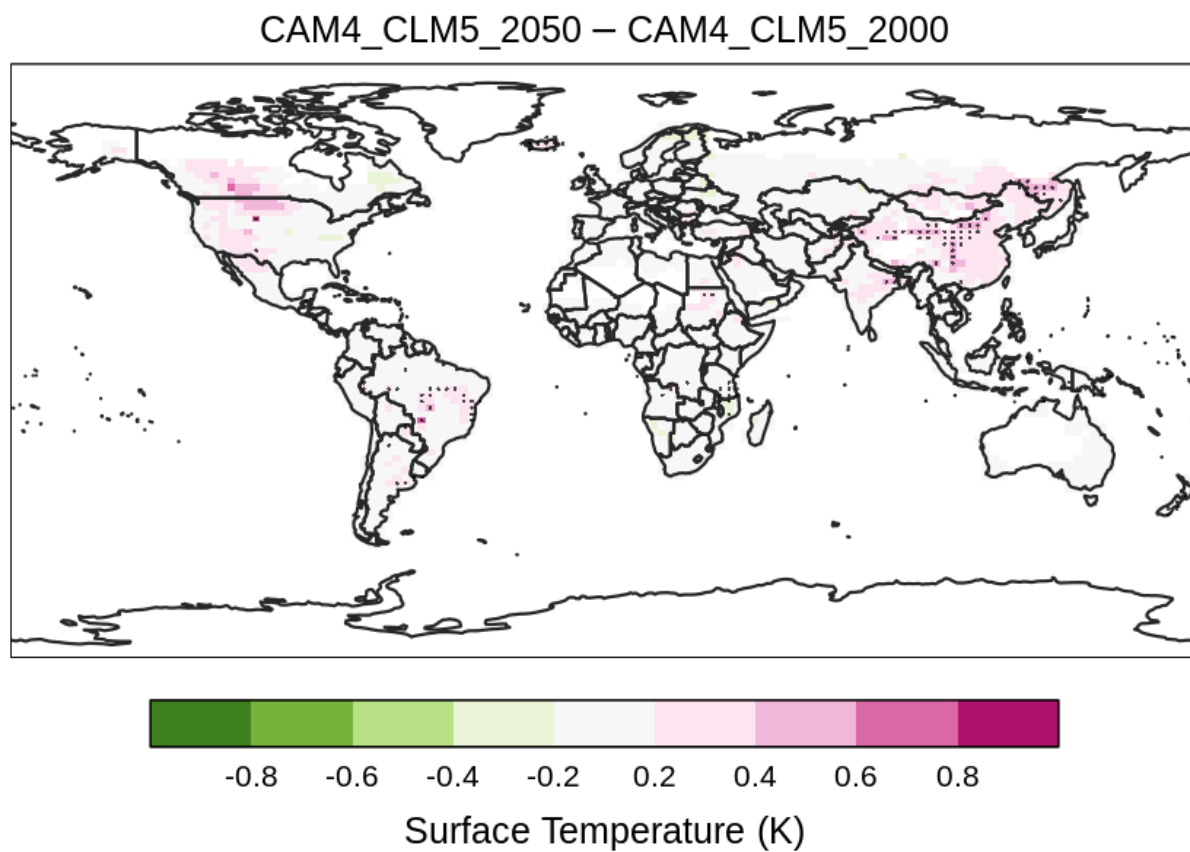


**Figure S6.** Contrasting the surface temperature (K). Overlaying black dots indicate grid-cells with a statistically significant difference under two-sample t-tests (i.e.,  $p < 0.05$ ) between corresponding simulations. Only results of grid-cells with croplands are shown.

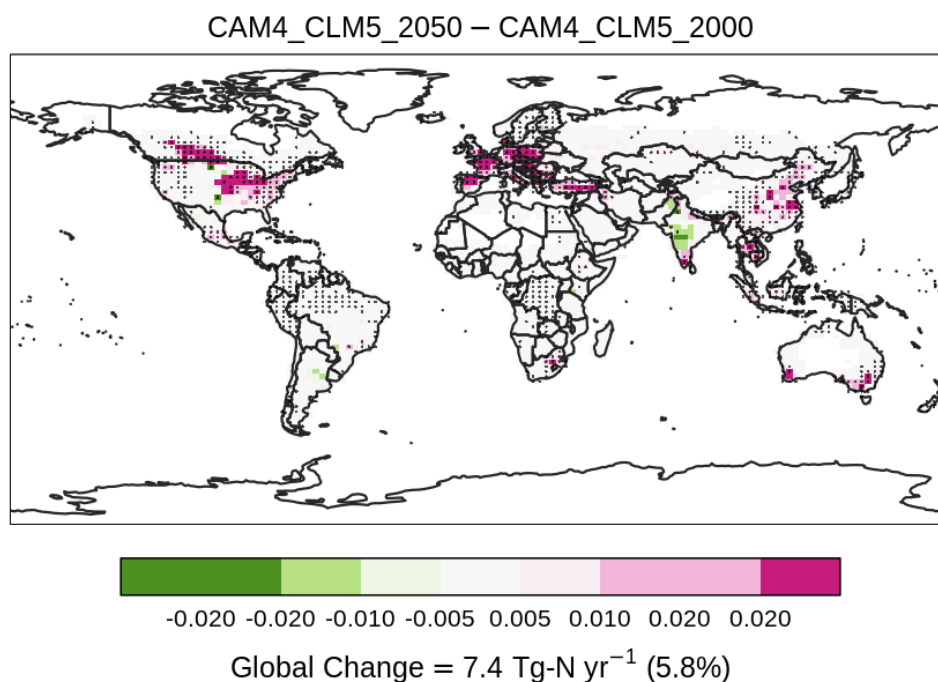


**Figure S7.** Changes in annual-total crop N uptake (Tg-N yr<sup>-1</sup>) after a 30% fertilization increase from [CAM4\_CLM5\_2000] to [CAM4\_CLM5\_2050]. Overlaying black dots indicate grid-cells with a statistically significant difference under two-sample t-tests (i.e.,  $p < 0.05$ ) between corresponding simulations. Color scales are saturated at respective values.

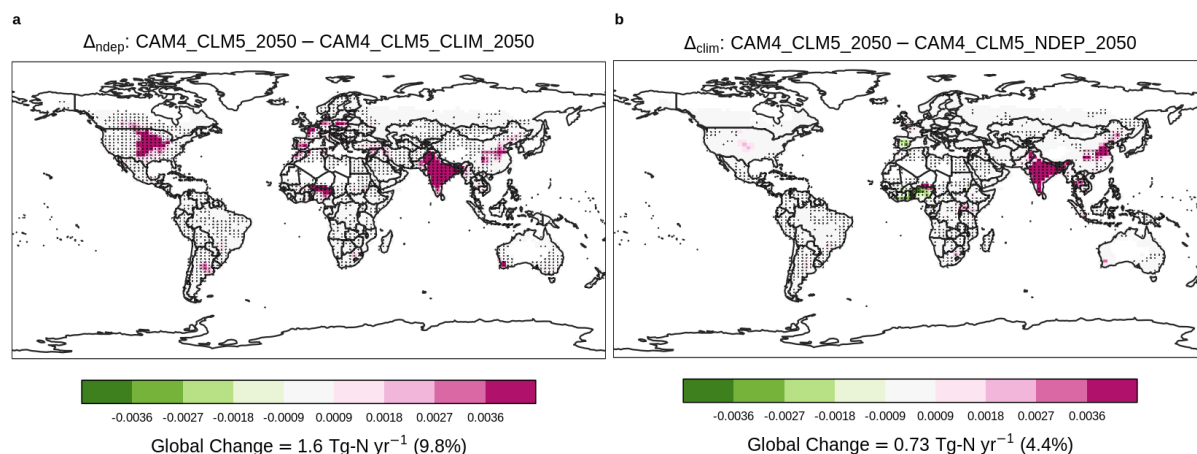


**Figure S8.** Contrasting the changes in nitrogen (N) deposition (Tg-N yr<sup>-1</sup>). Overlaying black dots indicate grid-cells with a statistically significant difference under two-sample t-tests (i.e.,  $p < 0.05$ ) between corresponding simulations. Only results of grid-cells with croplands are shown.

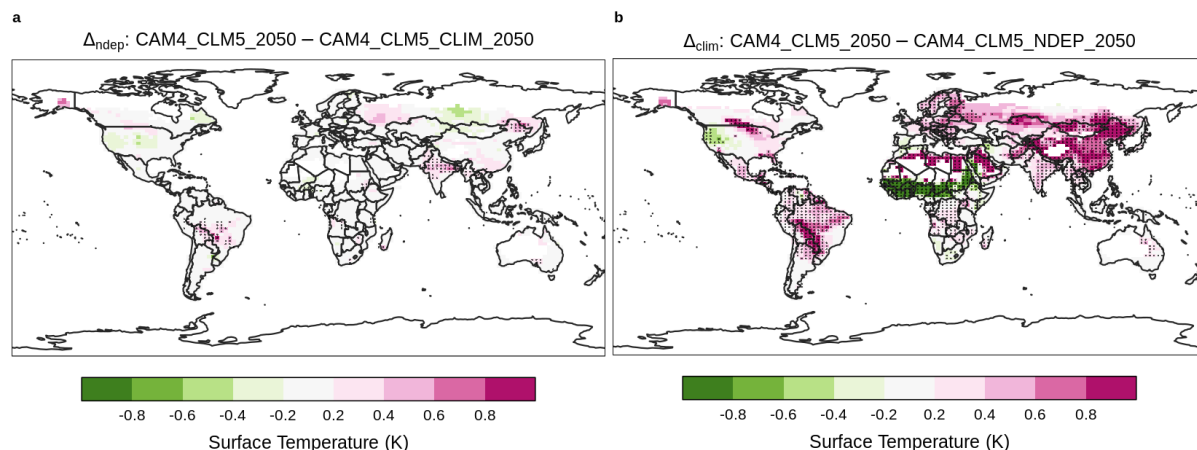


**Figure S9.** Contrasting the changes in annual-mean surface temperature (K). Overlaying black dots indicate grid-cells with a statistically significant difference under two-sample t-tests (i.e.,  $p < 0.05$ ) between corresponding simulations. Only results of grid-cells with croplands are shown.

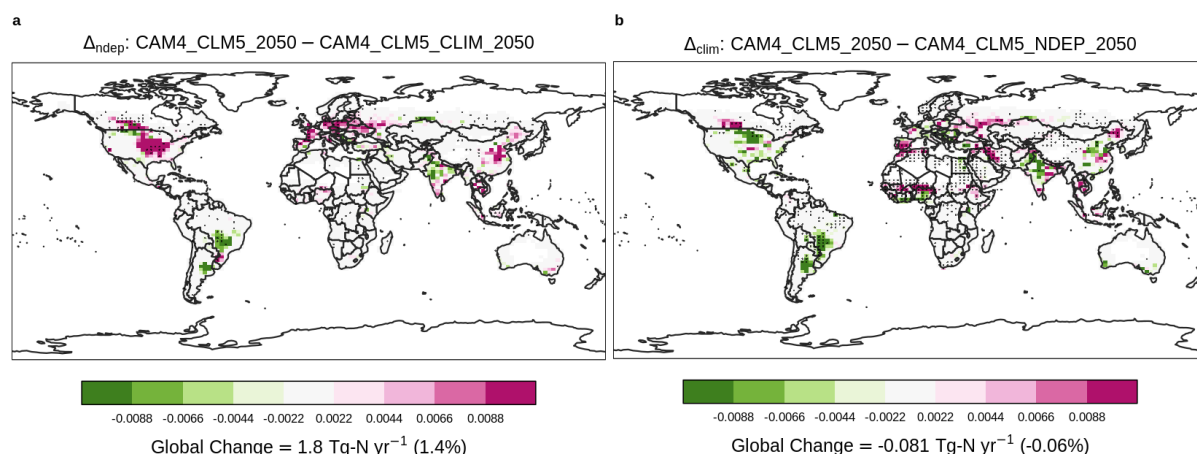


**Figure S10.** Contrasting the changes in plant nitrogen uptake (Tg-N yr<sup>-1</sup>). Overlaying black dots indicate grid-cells with a statistically significant difference under two-sample t-tests (i.e.,  $p < 0.05$ ) between corresponding simulations. Only results of grid-cells with croplands are shown.

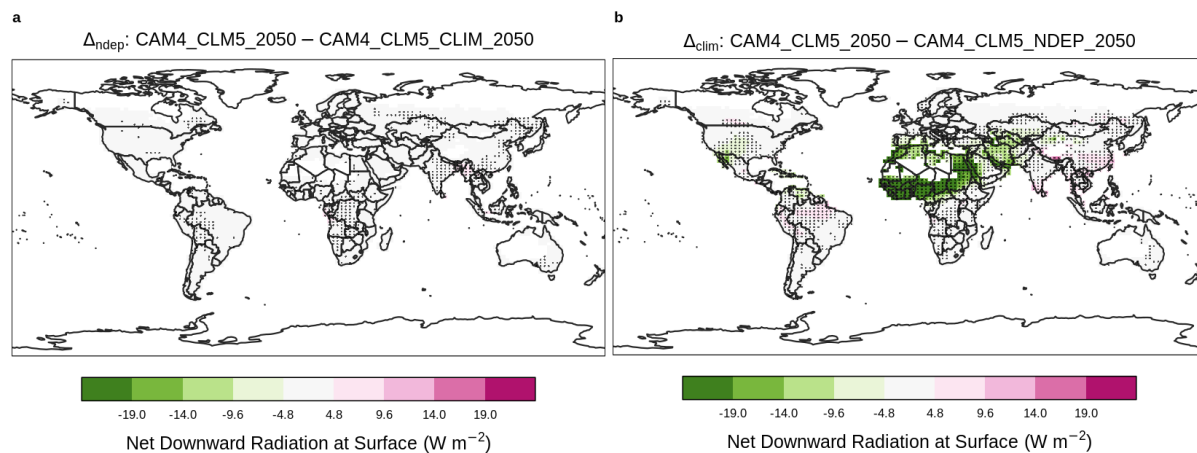


**Figure S11.** Contrasting the changes in annual-mean net downward radiation at surface ( $\text{W m}^{-2}$ ). Overlaying black dots indicate grid-cells with a statistically significant difference under two-sample t-tests (i.e.,  $p < 0.05$ ) between corresponding simulations. Only results of grid-cells with croplands are shown.

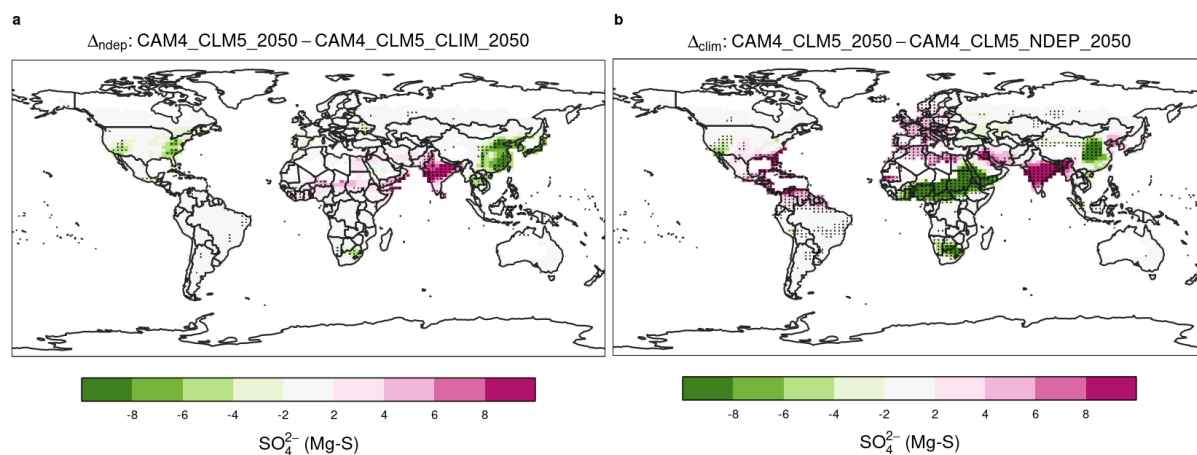


**Figure S12.** Contrasting the changes in annual-mean column burden of particulate sulfate. Overlaying black dots indicate grid-cells with a statistically significant difference under two-sample t-tests (i.e.,  $p < 0.05$ ) between corresponding simulations. Only results of grid-cells with croplands are shown.

## Reference

- 135 Bouwman, A. F., Lee, D. S., Asman, W. A. H., Dentener, F. J., Van Der Hoek, K. W., and Olivier, J. G. J.: A global high-resolution emission inventory for ammonia, 11, 561–587, <https://doi.org/10.1029/97GB02266>, 1997.
- Davidson, E. A. and Trumbore, S. E.: Gas diffusivity and production of CO<sub>2</sub> in deep soils of the eastern Amazon, 47, 550–565, <https://doi.org/10.1034/j.1600-0889.47.issue5.3.x>, 1995.
- 140 Del Grosso, S. J., Parton, W. J., Mosier, A. R., Ojima, D. S., Kulmala, A. E., and Phongpan, S.: General model for N<sub>2</sub>O and N<sub>2</sub> gas emissions from soils due to denitrification, 14, 1045–1060, <https://doi.org/10.1029/1999GB001225>, 2000.
- Li, C., Aber, J., Stange, F., Butterbach-Bahl, K., and Papen, H.: A process-oriented model of N<sub>2</sub>O and NO emissions from forest soils: 1. Model development, 105, 4369–4384, <https://doi.org/10.1029/1999JD900949>, 2000.
- 145 Li, C., Salas, W., Zhang, R., Krauter, C., Rotz, A., and Mitloehner, F.: Manure-DNDC: A biogeochemical process model for quantifying greenhouse gas and ammonia emissions from livestock manure systems, 93, 163–200, <https://doi.org/10.1007/s10705-012-9507-z>, 2012.
- Parton, W. J., Holland, E. A., Del Grosso, S. J., Hartman, M. D., Martin, R. E., Mosier, A. R., Ojima, D. S., and Schimel, D. S.: Generalized model for NO<sub>x</sub> and N<sub>2</sub>O emissions from soils, 150 106, 17403–17419, <https://doi.org/10.1029/2001JD900101>, 2001.
- Parton, W. J., Holland, E. A., Del Grosso, S. J., Hartman, M. D., Martin, R. E., Mosier, A. R., Ojima, D. S., and Schimel, D. S.: Generalized model for NO<sub>x</sub> and N<sub>2</sub>O emissions from soils , 106, 17403–17419, <https://doi.org/10.1029/2001jd900101>, 2004.
- 155 Wieder, W.: RegridDED Harmonized World Soil Database v1.2, <https://doi.org/10.3334/ornlDaac/1247>, 2014.
- Xu, R. and Prentice, I. C.: Terrestrial nitrogen cycle simulation with a dynamic global vegetation model, 14, 1745–1764, <https://doi.org/10.1111/j.1365-2486.2008.01625.x>, 2008.
- 160 Zhao, Y., Zhang, L., Tai, A. P. K., Chen, Y., and Pan, Y.: Responses of surface ozone air quality to anthropogenic nitrogen deposition in the Northern Hemisphere, 17, 9781–9796, <https://doi.org/10.5194/acp-17-9781-2017>, 2017.